Low impedance and highly transparent microelectrode arrays (MEA) for in vitro neuron electrical activity probing

Anna Susloparova, Sophie Halliez, Séverine Begard, Morvane Colin, Luc Buée, Sébastien Pecqueur, F. Alibart, V. Thomy, S. Arscott, Emiliano Pallecchi, et al.

Low impedance and highly transparent microelectrode arrays (MEA) for *in vitro* neuron electrical activity probing.

Anna Susloparova[1], Sophie Halliez[2], Séverine Begard[2], Morvane Colin[2], Luc Buée[2], Sébastien Pecqueur[1], Fabien Alibart[1,3], Vincent Thomy[1], Steve Arscott[1], Emiliano Pallecchi[1], Yannick Coffinier[1]

1) Univ. Lille, CNRS, Centrale Lille, Univ. Polytechnique Hauts-de-France, UMR 8520 - IEMN, F-59000 Lille, France. Email: yannick.coffinier@univ-lille1.fr

2) Univ. Lille, Inserm, CHU Lille, U1172 - LilNCog - Lille Neuroscience & Cognition, F-59000 Lille, France

3) Laboratoire Nanotechnologies & Nanosystèmes (LN2), CNRS, Université de Sherbrooke, J1X0A5, Sherbrooke, Canada.

Abstract

In this study, we present the microfabrication and characterization of a transparent microelectrode array (MEA) system based on PEDOT:PSS for electrophysiology. The influence of the PEDOT:PSS electrode dimensions on the impedance was investigated and the stability over time under physiological environment was demonstrated. A very good transparency value was obtained—our system displaying one of the best impedance and transmittance values when compared to other transparent MEAs. After biocompatibility validation, we successfully recorded spontaneous neuronal activity of primary cortical neurons cultured over 4 weeks on the transparent PEDOT:PSS electrodes. This work shows that microelectrodes composed of PEDOT:PSS are very promising as a new tool for both electrophysiology and fluorescence microscopy studies on neuronal cell cultures.

Keywords

microelectrode array, transparent electrodes, PEDOT:PSS, low impedance, neuronal network activity

1. Introduction

Microelectrode arrays (MEA) are recognized as standard tools allowing recording *in vitro* biological activity of neuronal cells [1,2], cardiac cells [3,4] and from brain slices [5,6]. Recently, integrated tools combining both electro- and optophysiology (calcium or voltage sensitive imaging) have gained great interest for a better understanding of physiological phenomena within neural networks. Further development of transparent microelectrodes is

required since they enable simultaneous electrophysiology and optical imaging (i.e. high-resolution fluorescence imaging in tandem with transmission microscopy). Biocompatible, transparent microelectrodes have been demonstrated using a number of means. Thin titanium nitride (TiN) electrodes (30 μm in diameter) were fabricated by sputtering with an electrode surface impedance below 175 MΩ μm^2 [7] and a transmission at visible wavelengths of 50% [8]--or by atomic layer deposition (ALD) with an electrode surface impedance from 360 to 420 MΩ μm^2 and a transmission at visible wavelengths of 19–45% [9]. Due to the trade-off between metal transparency and metal conductance affecting optical transmission and electrode impedance (i.e. decreasing the metal thickness to increase transparency leads to an increase in electrical impedance due to an increase of resistance), development of both transparent and conductive materials is needed [10]. In previous publications, transparent MEAs based on indium tin oxide (ITO) with transmission at visible wavelengths of 80% [11] and graphene with transmission at visible wavelengths of 90% [12-14] were proposed. However, the impedance values of transparent ITO and graphene electrodes cannot compete with standard non-transparent MEA devices with TiN electrodes. As a comparison, the surface impedance at 1 kHz of 30 μm diameter TiN electrodes was below 70 MΩ μm^2 [7], whilst it was 7500 MΩ μm^2 for 200 μm diameter graphene electrodes [14] and 1250 MΩ μm^2 for 80 μm diameter ITO electrodes [15]. In addition, miniaturization of microelectrodes to match single neuronal cells dimensions (a few tens of μm) also affects electrodes impedance [16], due to a decrease in the interfacial capacitance which is directly correlated with the microelectrode area [5]. Therefore, manufacturing small electrodes with high transparency whilst keeping the impedance as low as possible cannot be solved solely by geometrical optimization of the electrodes—and other material solutions are required.

In the past decades, conducting polymers have attracted great interest and is currently a buoyant field of research due to their lower microelectrode impedance compare to inorganic materials [17]. Of particular interest for the development of transparent and low impedance MEA electrodesis Poly(3,4-ethylenedioxythiophene) doped with poly(styrene sulfonate) (PEDOT:PSS) which is considered as a very promising candidate. In addition to chemical stability [18] and biocompatibility [19], PEDOT:PSS displays good optical transmittance (> 90%) and high conductivity (>10^3 S cm^{-1}) [20]. Also, a combination of both electronic and ionic conductivity in the bulk of the material provides an additional degree of freedom to be able to optimize its capacitance (i.e. volumetric capacitance rather than surface capacitance).

PEDOT:PSS has been already used to produce low impedance microelectrodes by coating such materials as gold [21,1,5,4,22] or platinum [17]—as well as to reduce the impedance of graphene microelectrodes [3]. Whereas in previous publications, PEDOT:PSS was used to improve the recording performance of the opaque as well as transparent microelectrodes, in this

work, PEDOT:PSS will be used as the sole conductive element of the electrodes. Although fabrication of flexible PEDOT:PSS based MEAs by means of inkjet–printing [23] with surface impedance of 1380 MΩ μm^2 at 1 kHz has been demonstrated, the main issues of this process were linked to the electrode dimension (diameter of 300 μm) as well as the resolution and reproducibility of the patterns [23].

The goal of this work is to develop small, biocompatible, transparent electrodes with low impedance and high transparency. The approach used in this work solves the main challenges of dimension/impedance and transparency/impedance by microfabrication of the microelectrodes from PEDOT:PSS material. For the first time, the fabrication of transparent electrodes made of PEDOT:PSS was demonstrated. A PEDOT:PSS solution is mixed with ethylene glycol, dodecyl benzene sulfonic acid (DBSA) and 1wt.% of (3-Glycidyloxypropyl)trimethoxysilane (GOPS). Ethylene glycol is added to enhance the conductivity of PEDOT:PSS, DBSA helps to adjust the surface tension and GOPS enhances the stability of PEDOT:PSS in aqueous environments [5]. From now on, this mixture will be denoted as PEDOT:PSS for simplicity since it is not deposited on either metallic electrodes or other conductive material such as ITO or even don't mixed with carbon nanotubes or graphene. The electrical characteristics of the electrodes and their robustness/stability were assessed over time by long term electrical impedance measurements. The biocompatibility of the different materials of the MEA device was also validated. Neural cells culture activity was demonstrated with electrodes composed of pure PEDOT:PSS. The work shows that microelectrodes made of PEDOT:PSS are very promising for both electrophysiology and optical characterization (fluorescence)/stimulation (optogenetics) experiments on neurons.

2. Material and methods

MEA fabrication process

A schematic representation of the microfabrication process of the MEA devices with PEDOT:PSS electrodes is shown in Fig. 1a-f. Briefly, the process involves the patterning of gold contact pads and tracks as well as the patterning of the PEDOT:PSS microelectrodes onto a glass substrate (1 mm thick). Parylene C is used as an insulating layer on the circuit where required. The specific details of the fabrication process are presented in supplementary material. Fig. 1g presents a photograph of a fabricated MEA device complete with a cell culture chamber. Fig. 1h show a photograph (plus zoom) of the PEDOT:PSS electrodes, the openings in the Parylene, and the gold contact lines.

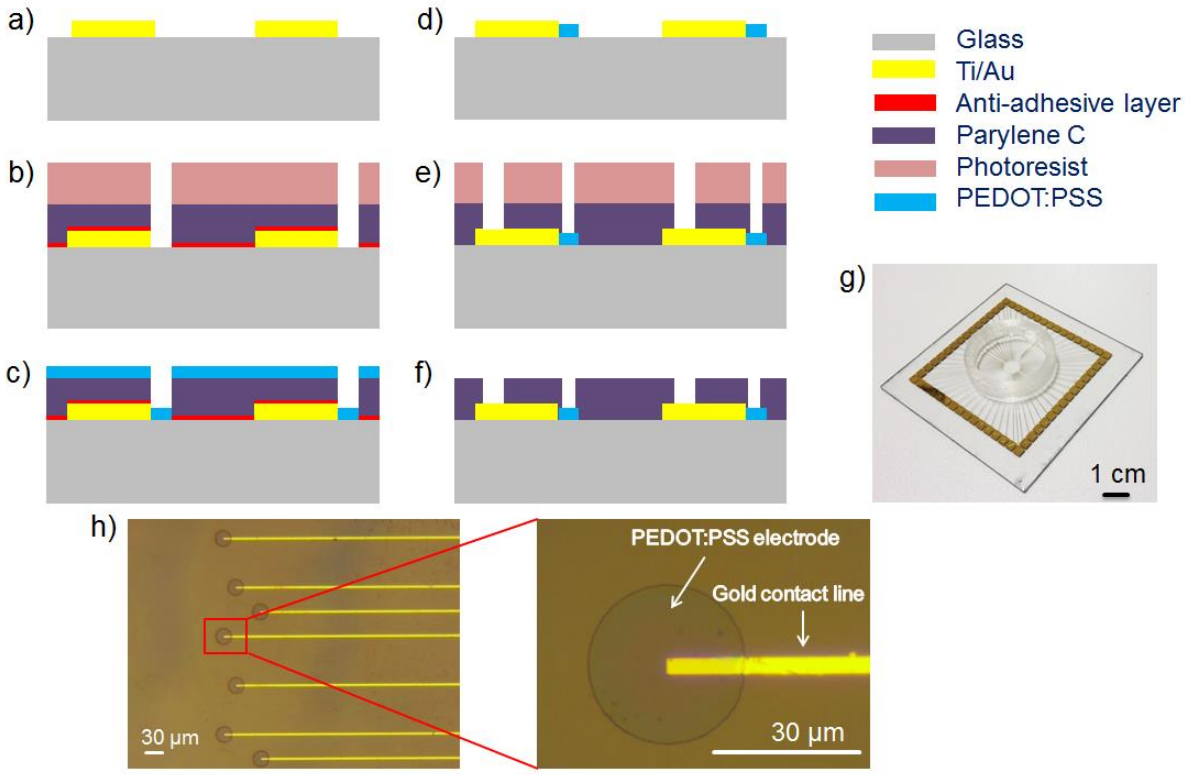

Fig. 1 Schematic representation of the fabrication process of the MEA devices with electrodes from pure PEDOT:PSS (a) patterning of the gold contact pads and interconnects onto a glass wafer *via* Ebeam lithography and lift-off (b) spin-coating of an anti-adhesive layer, deposition of 2 µm thick parylene C layer, spin-coating of the photoresist and openings of the microelectrodes by 2nd Ebeam lithography followed by oxygen plasma etching (c) removal of the photoresist and spin-coating of the PEDOT:PSS solution (d) peeling-off the parylene C sacrificial layer (e) deposition of the second 2 µm thick parylene C layer, spin-coating of the photoresist and openings of the contact pads and electrodes by 3rd Ebeam lithography step and oxygen plasma etching (f) removal of the photoresist (g) A photograph of a fabricated MEA device with gold contact pads and tracks, PEDOT:PSS microelectrodes in the center and the cell culture chamber made of PDMS on top. h) Microscopic image of the PEDOT:PSS microelectrodes. The thickness of spin-coated PEDOT:PSS layer is 200 nm.

3 Results and discussion

The MEA device consists of 59 round recording electrodes and one large reference electrode (740 µm in diameter) (Fig S1 in supplementary material). The dimensions of the device (49 × 49 × 1 mm^3), the configuration of the contact pads, and of the internal reference electrode are compatible with commercial MEA-System (MEA2100-System, Headstage for 2 MEAs with 60 electrodes, Multi Channel Systems). The surface of the patterned microelectrodes was characterized by means of atomic force microscopy (AFM) as well as scanning electron microscopy (SEM) (Fig. S2 in supplementary material).

3.1 Electrical characterization of the MEA devices

MEA require low impedance to achieve a high signal-to-noise ratio. The MEA devices with PEDOT:PSS electrodes were characterized using impedance spectroscopy (KEYSIGHT E4990A Impedance Analyzer). The measurements were performed in presence of phosphate buffer saline (PBS) solution by applying a 100 mV sine wave with the frequency varied from 20 Hz to 1 MHz.

3.1.1 Influence of electrode diameter

Firstly, the influence of the electrode size on the surface impedance was investigated. Fig. 2a compares the impedance spectra measured on the same MEA device with the same thickness of PEDOT:PSS electrodes (200 nm) but with different diameters (10 and 30 µm). By comparing the values of surface impedance at 1 kHz, the typical frequency used for neuronal signals recording, it was observed that electrodes having a larger diameter have a lower surface impedance value--due to expected higher interfacial capacitance [5]. The surface impedance values (mean ± standard deviation) at 1 kHz were 35.4 ± 8MΩ µm^2 for electrodes with a diameter of 10 µm and 33 ± 2.6 MΩ µm^2 for electrodes with a diameter of 30 µm, respectively. The values were obtained by averaging the impedance spectra of 20 electrodes for each diameter. The similar dependence of the impedance on the electrode size was demonstrated for the commercial MEA devices. As a comparison, the surface impedance of TiN electrodes ranges between 21.2 – 35.3 MΩ µm^2 for electrodes of 10 µm in diameter and 19.6 – 31.4 MΩ µm^2 for electrodes of 30 µm in diameter [24]. The crossing effect of the impedance spectra at around 4 kHz could be mostly attributed to post-measurement normalization of the impedance with area that induces additional error bars (i.e. electrode size accuracy).

3.1.2 Influence of PEDOT:PSS thickness

The influence of the thickness of the PEDOT:PSS electrodes on the surface impedance was investigated. Fig. 2b shows the impedance spectra of PEDOT:PSS electrodes having the same sizebut with different thicknesses. A significant surface impedance decrease for the thicker PEDOT:PSS electrodes was observed due to a corresponding capacitance increase [25] (Rivnay et al., 2015). For example, the surface impedance value at 1 kHz for electrodes having a diameter of 30 µm and a PEDOT:PSS thickness of 100 nm is 95.2 ± 3.7 MΩ µm^2, whilst the surface impedance value for the PEDOT:PSS layer having a thickness of 200 nm is 33 ± 2.6 MΩ µm^2, respectively (Fig. 2b). This effect can be explained by the dependence of the capacitance on the thickness. Indeed, an increase of the PEDOT:PSS thickness is correlated with the increase of PEDOT:PSS volume and corresponds to the increase of capacitance, which, as a consequence, leads to a decrease of the surface impedance [25]. A similar dependence of

surface impedance to the thickness of the electrode material was already shown by Kshirsagar et al. [3] who demonstrated that increasing the PEDOT:PSS layer thickness (electrodeposited by different time durations) led to a decrease of the impedance value. As a comparison, the impedance of a PEDOT:PSS layer electrodeposited during 0.2 sec is around 700 kΩ whilst those of PEDOT:PSS layers electrodeposited during 10 sec is around 50 kΩ—the thickness of the PEDOT:PSS layer is proportional to the deposition time [3].

The low frequency part of the curves is mostly related to the electrode impedance contribution whereas the high frequency part is mostly related to the electrolyte impedance. Since the measured electrode impedance was normalized to the surface, there is small impedance differences at low frequencies. In the case of thickness, there is no normalization of the thickness—so the impedance differences are very pronounced at low frequencies. Due to the different distances between electrodes and the reference electrode, the electrolyte impedance can vary from electrode to electrode, which leads to the impedance differences at high frequencies.

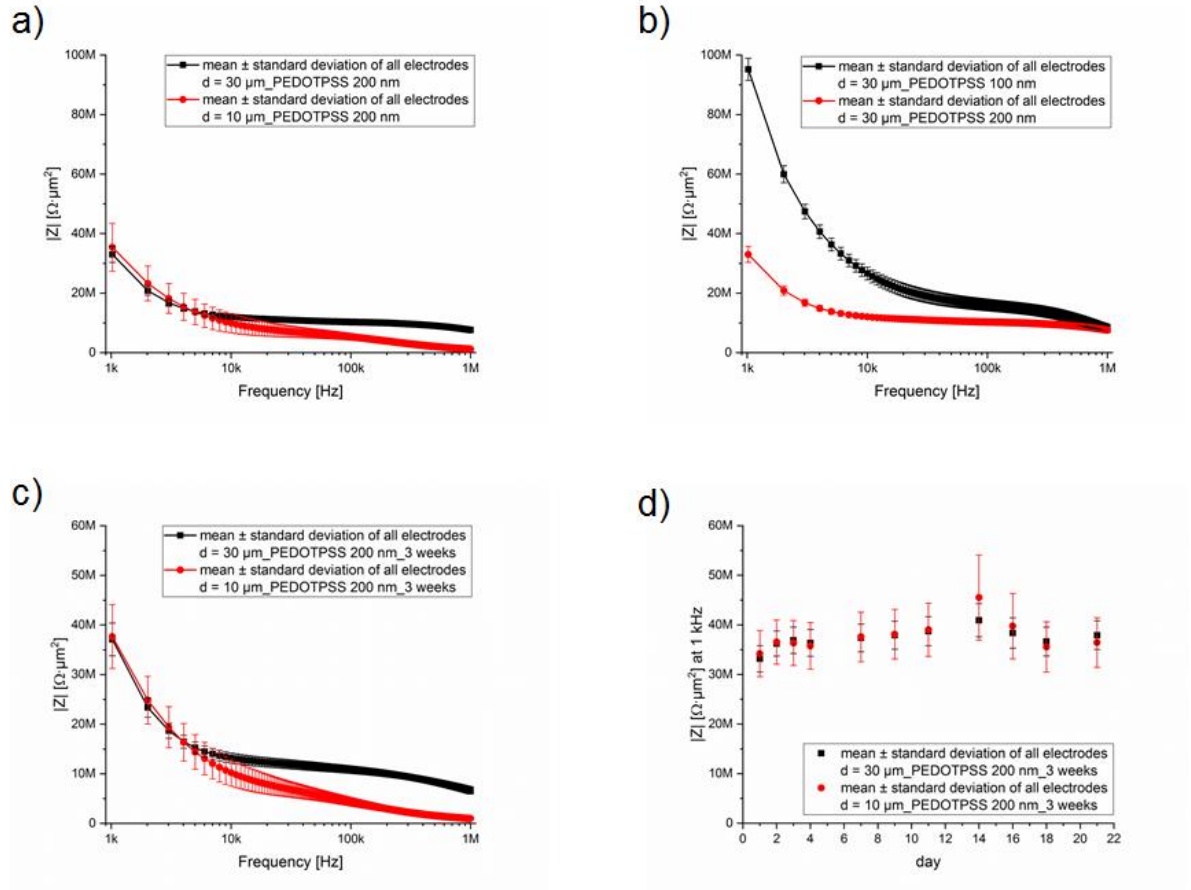

Fig. 2 (a) Influence of electrode diameter on surface impedance. The impedance spectra measured for PEDOT:PSS electrodes (200 nm thick) for different electrode sizes (10 and 30 µm). (b) Influence of PEDOT:PSS thickness on surface impedance. The impedance spectra measured for PEDOT:PSS electrodes (30 µm in diameter) for different thicknesses (100 and 200 nm). Long-term stability measurement done in PBS solution over 3 weeks. (c)

Averaged impedance spectra measured during 3 weeks of all electrodes with a diameter of 10 and 30 µm on the same MEA device with PEDOT:PSS thickness of 200 nm. (d) Surface impedance values at 1 kHz over 22 days for all electrodes (10 and 30 µm of diameter).

3.1.3 Electrode to electrode impedance variability

Variation àof the surface impedance value from electrode to electrode on the same device is crucial to assess to detect the similar extracellular signals in neurophysiology. The surface impedance values (mean ± standard deviation) at 1 kHz were 35.4 ± 8MΩ µm^2 for electrodes with a diameter of 10 µm and 33 ± 2.6 MΩ µm^2 for electrodes with a diameter of 30 µm, respectively. The values indicate a small variation from electrode to electrode on the same device and thus validate the good quality of the fabrication process. Moreover, the slight variation ofsurface impedance values from electrode to electrode are comparable to those from electrodes made of other materials. Aa a comparison, the surface impedance values (mean ± standard deviation) at 1 kHz of 24 electrodes with a diameter of 30 µm 37 ± 3.3 MΩ µm^2, 14 ± 1.3 MΩ µm^2 and 11.5 ± 0.7 MΩ µm^2, made of TiN, gold coated with PEDOT and gold coated with PEDOT-CNT, respectively [4].

3.1.4 Stability of PEDOT:PSS *electrode impedance*

Next, the stability of PEDOT:PSS MEA devices for long-term experiments was studied. The electrical performance of the electrodes needs to be stable over time because typical neurons' cell cultures start exhibiting synchronized burst events around 3 weeks of DIV culture [1]. For example, commercial MEAs with TiN electrodes (Multi Channel System) are stable for long-term experiments (up to several weeks or even month) [25]. In order to investigate the stability of our MEA devices, their impedances were measured during several weeks (3 – 4 measurements per week) in a PBS solution. Between the measurements, the MEA devices were stored in deionized water in order to avoid an increase of impedance.

Fig. 2c shows the impedance spectra obtained by averaging several impedance spectra measured in a PBS solution during 3 weeks for electrodes having a diameter of 10 and 30 µm on the same device with a PEDOT:PSS thickness of 200 nm. The surface impedance values (mean ± standard deviation) at 1 kHz were 37.6 ± 6.4 MΩ µm^2 and 37.1 ± 3.3 MΩ µm^2 for electrodes with a diameter of 10 and 30 µm, respectively.

Fig. 2d presents the evolution over time of the impedance values at 1 kHz for electrodes with a diameter of 10 and 30 µm. The first impedance measurement was performed immediately after fabrication of the device. The next measurement of the surface impedance was performed on the next day after storing overnight the device in deionized water. The increase of the surface impedance can be explained by a stabilization of PEDOT:PSS and by the removal of any excess

of low molecular weight compounds from PEDOT:PSS dispersion [1]. The surface impedance values subsequently measured during a 3 week period were almost at the same level. The insignificant change in impedance after measurements during 3 weeks demonstrates the stability of our devices and validity for long-term experiments.

Mean and standard deviation values at 1 kHz over 3 weeks measurements for electrodes with a diameter of 10 and 30 µm, are presented in tables S2 and S3, respectively.

A similar impedance behaviour was measured for the thinner PEDOT:PSS electrodes (i.e. 100 nm thick) during 10 weeks. The surface impedance value (mean ± standard deviation) at 1 kHz was 122.2 ± 15.7 MΩ μm^2 (Fig. S5 in supplementary material).

Following the characterization, the following parameters (30 µm diameter and with the PEDOT:PSS thickness of 200 nm) were finally chosen and used for the fabrication of the MEA devices intended for the recording of the electrical neuronal activity. In biological applications, and notably for neuron activity measurements, data confidence is crucial, and so reliable MEA devices are mandatory. In the following section, we have tested several devices and have investigated the impedance variation from device to device.

3.1.5 Impedance variation from device to device

Fot this part of the study, six MEA devices with electrodes having a diameter of 30 µm and a PEDOT:PSS thickness of 200 nm have been fabricated and characterized. All devices were entirely fabricated separately from each other by using a freshly prepared PEDOT:PSS mixture for spin-coating. The values shown in Fig. 3 were obtained by averaging the impedance values at 1 kHz of all electrodes of each device. The averaging values of surface impedance at 1 kHz are in the range of 24 – 35 MΩ μm^2.

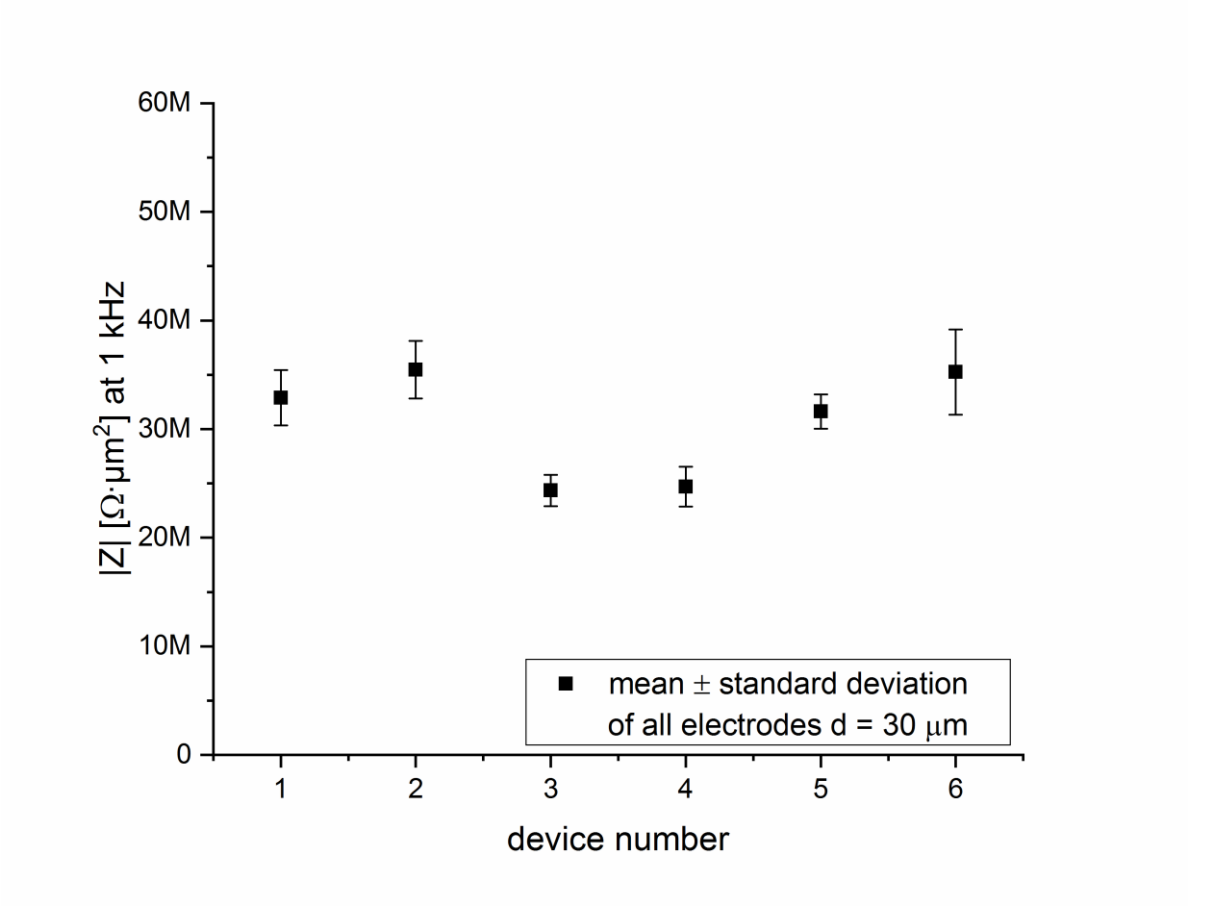

Fig. 3 The device to device reproducibility. Averaging the surface impedance values at 1 kHz of all electrodes with a diameter of 30 µm and the PEDOT:PSS thickness of 200 nm for 6 different MEAs.

The impedance values of PEDOT:PSS electrodes are comparable to the impedance values of state-of-the-art MEA devices (Table 1).

Electrode dimension	**Electrode material**	**|Z| [kΩ] at 1 kHz**	**|Z| [MΩ µm²] at 1 kHz**	**Transmission [%]**	**Reference**
10 × 10 µm²	Ti/Au +PEDOT:PSS (350 nm)	35	3.5	Opaque	[1]
d = 50 µm	Ti/Au +PEDOT:PSS	20	39	Opaque	[17]
20 × 20 µm²	Ti/Au +PEDOT:PSS (380 nm)	23	9.2	Opaque	[5]
d = 30 µm	Au +PEDOT (247 ± 33 nm) Au +PEDOT-CNT (352 ± 27 nm)	20.0 ± 1.9 16.2 ± 1.1	14.1 ± 1.3 11.4 ± 0.8	Opaque	[4]

d = 30 µm	TiN	< 100	21.2 – 35.3	Opaque	Multi Channel Systems
d = 10 µm	TiN	250 – 400	19.6 – 31.4	Opaque	Multi Channel Systems
d = 30 µm	ALD TiN	510 – 590	360-390	18 – 45	[9]
d = 30 µm	Transparent TiN	< 250	177		Multi Channel Systems
d = 200 µm	graphene	243 ± 6	7650 ± 3	90	[14]
d = 30 µm	Graphene/ PEDOT:PSS	166 ± 13	117 ± 9	84 ± 4	[3]
d = 80 µm	ITO	250	1250	80	[15]
d = 30 µm	PEDOT:PSS (200 nm)	46.5 ± 3.7	32.9 ± 2.6	93	**this work**
d = 10 µm	PEDOT:PSS (200 nm)	433.2 ± 58.5	35.4 ± 8	93	**this work**

Table 1 Comparison of the impedance values at 1 kHz and transmission values of the electrodes from different materials.

3.1.6 Transmission measurement

In order to combine both electrophysiology measuements and the ablity of optical microscopy observation, we aimed to fabricate both transparent and low impedance electrodes (32.9 ± 2.6 MΩ µm^2 at 1 kHz for 30 µm diameter electrodes). The average transmission at visible wavelengths was 97% and 93% for plain PEDOT:PSS layers deposited by spin-coating on glass slides with thickness of 100 nm and 200 nm, respectively (Fig. S6 in supplementary material). As a comparison, a transparency of 84% was obtained for graphene/PEDOT:PSS-based MEA– but with higher surface impedance value of 117.3 ± 9.2 MΩ µm^2 at 1 kHz (30 µm diameter) [3] while an 80% transparency was obtained using ITO-based MEAs [26] with a surface impedance value of 1250 MΩ µm^2 (80 µm diameter) [9]. Table 1 and Fig.S7 (supplementary material) shows impedance values (MΩ µm^2) and optical transmissions (%) of our MEA compared to other transparent MEA described in literature and to non-transparent commercial TiN based MEA.

3.2 Biocompatibility assessment

The biocompatibility of all MEA device materials intended to be in contact with cells (PDMS, PEDOT:PSS and Parylene) was tested by performing metabolic activity assays that will directly reflect the living cell numbersand cell death assays. Rat cortical cells grown on PDMS, PEDOT:PSS and Parylene on top of PEDOT:PSS were compared to cells grown on glass after 7, 14, 22 and 28 days of culture *in vitro* (DIV)--results are shown in Fig. 4 and Tables S4 and

S5 in supplementary material). The mean metabolic activity of cells grown on PDMS was significantly lower at 14, 22 and 28 DIV—and the cell death significantly increased at 22 and 28 DIV. This indicates a biocompatibility clearly inferior to the biocompatibility of glass. However, in our final device, as only the walls of the well are made of PDMS, we assumed this would not have a significant impact on the results. The mean metabolic activity of cells grown on PEDOT:PSS was significantly lower at 7 and 14 DIV. It was also lower at 22 and 28 DIV but no significant difference was observed. The cell death was significantly increased only at 7 DIV. This suggests that PEDOT:PSS does not promote cell adherence when compared to glass but, once cells have adhered to it, their viability is quite similar to cells grown on glass. This would explain both the reduced number of living cells observed right after cell seeding and the similar mortality rate compared to control observed at more advanced times. Regarding the possible leaching of toxic additives mixed with the PEDOT:PSS solution (ethylene glycol, DBSA and GOPS), as we did not change the cell culture medium during the entire culture (28 DIV), we assume the sensitivity of our assay to such leaching is quite high. In that case, even a slight leaching would be expected to impact cell viability at some point through accumulation of these additives in the medium. Yet, we did not observe lower cell viability at advanced time points ruling out any leaching-induced toxicity.

The mean metabolic activity of cells grown on parylene was mildly lower through the 4 weeks of culture but the reduction was only found to be significant at 14 DIV. Moreover, the cell death was never found to be significantly increased. This indicates that parylene biocompatibility is only slightly lower than glass biocompatibility. This slight difference is probably due to a reduced cellular adherence during seeding process rather than to an increased cellular death. Altogether, these results indicate that our final device will allow the growth of neuronal cells although a slight reduction in the number of living cortical cells could be expected.

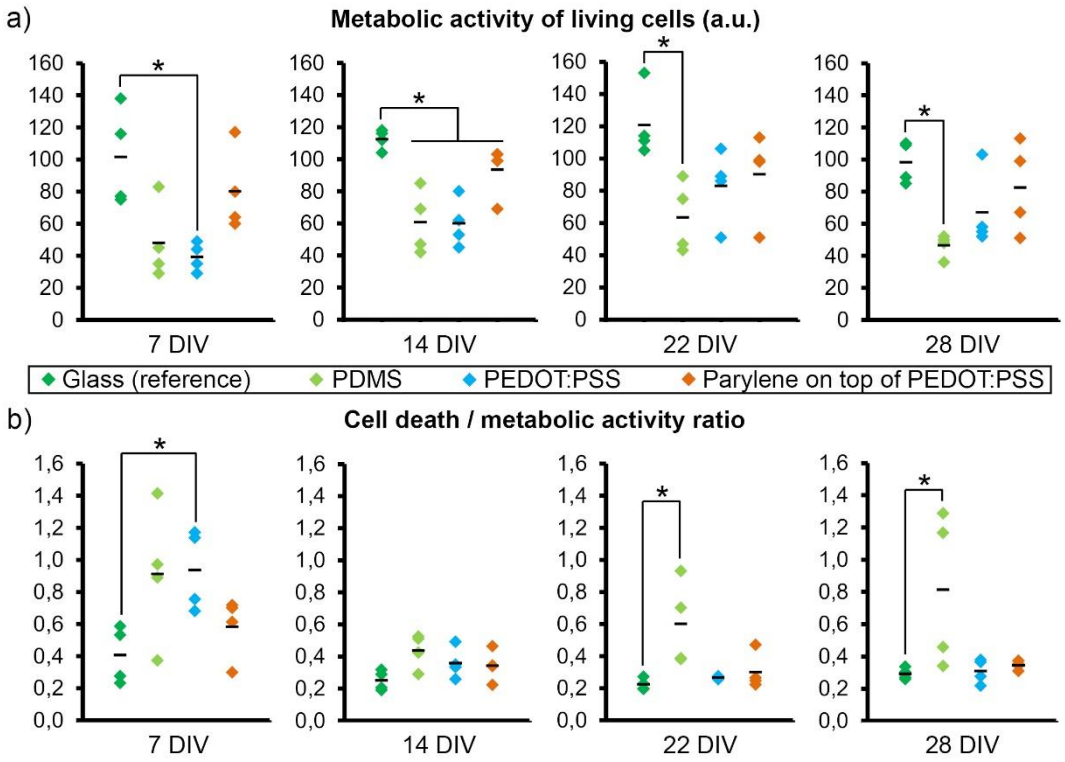

Fig. 4 Biocompatibility assessment of materials composing the MEA device. The biocompatibility of PDMS, PEDOT:PSS and parylene was compared to glass biocompatibility through metabolic activity assays (a) and death cell assays (the ratio of cell death on metabolic activity is presented in b). Rat primary cortical cells were seeded on the different substrates and tests were performed after 7, 14, 22 and 28 DIV. Mean values are indicated in black. n=4 biological replicates for each condition. Significant differences between results obtained for cells grown on glass and results obtained for other substrates were examined using the nonparametric Mann-Whitney and Wilcoxon tests (*:p<0.05).

3.3 Cell culture on the PEDOT:PSS electrodes

We and others have characterized extensively cortical cell cultures using MEA technology and immunofluorescence stainings [27,28]. Typically, our cultures start exhibiting spontaneous globally-synchronized burst events after around 3 weeks of culture (Fig. S9 in supplementary material). Based on these observations, we chose to follow the establishment of functional neural networks from dissociated cortical cells during 4 weeks in order to provide a proof-of-concept for the fabrication of biocompatible electrodes using PEDOT:PSS. A cortical cell culture was established on a MEA device with PEDOT:PSS electrodes . Spontaneous neuronal cell activity was recorded after 14, 21 and 28 DIV (Fig. 5, culture 1, Tables S6-S8 in supplementary material). As commercial MEAs are reusable, we investigated to see if the PEDOT:PSS MEA could also sustain a standard cleaning method in order to be reused

afterwards. After culture 1, the cells and extracellular proteins were washed out from the MEA device using an anionic detergent with protease enzyme. The electrode impedance was checked out and no change was observed (data not shown). We then established a new cortical cell culture and new recordings were performed (Fig. 5, culture 2, Tables S6-S8 in supplementary material). Several parameters (number of active electrodes, spike and burst frequencies, burst duration and number of spikes per burst) were extracted from the two series of recordings and compared to data obtained with control cortical cell cultures established on commercial MEAs with electrodes from TiN (Fig. 5, commercial MEAs n = 3, Tables S6-S8 in supplementary material). After 3 weeks of culture, the majority of the PEDOT:PSS electrodes allow recording neuronal activity (Fig. S9a in supplementary material) that was found comparable to control cultures (Fig. 5). The increased firing rate and the network activity synchronization (Fig. 5e and 5f) observed over time show proper maturation of the neural network as expected. However, cultures established on commercial MEAs seem to reach a high level of synchronization sooner (Fig. 5e). One can note that the baseline noise level observed during neuronal activity recording is smaller with the PEDOT:PSS electrodes (around 9 µV) when compared to TiN electrodes from commercial MEAs (around 15 µV) (Fig. S9b in supplementary material) suggesting a higher signal-to-noise ratio and therefore a better ability to detect extracellular activity. The MEA device with PEDOT:PSS electrodes detects lower intensity signals than commercial MEAs and this for every stage assayed (Tables S6-S8 in supplementary material). Further experiments are needed to determine if the apparent delayed in synchronization we observed (Fig. 5e) is related to a wider range of detection and therefore to improved technical performances (depending of the algorithm and method selected to quantify activity correlation) rather than to a biological cause (i.e. differences in the neural network maturation rate). Usually, synchronised burst events correspond to high intensity signals, so signals easily detectable. Depending of the network structure and positioning of the electrodes, non-synchronised events correspond partially to high intensity signals and partially to lower intensity signals and therefore are partially easily detectable, partially less easily detectable. Lowering the detection threshold will not modify the occurrence of synchronised events *per se* but depending on the network structure and positioning of the electrodes, this can allow increasing the detection of non-synchronised events and therefore decreasing the proportion of synchronised events. Alternatively, although similar numbers of cortical cells had been seeded on the different types of MEAs, we cannot rule out that a slightly lower number of cells adhered to MEA device with PEDOT:PSS electrodes as suggested by our biocompatibility study. As cell density impacts network maturation [28], this could be also explained by the synchronization delay. In that case, a slight increase in cell concentration at the seeding step would solve the problem. Both explanations are not mutually exclusive.

To image live neurons on top of the PEDOT:PSS electrodes, we used a fluorescent probe that selectively labels living neurons. After one month of culture, fluorescent-positive living neurons were perfectly visible on top of the electrodes and everywhere on the recording area (Fig. 5). This, in combination with the neuronal activity recordings, provides proof-of-concept for the fabrication of a biocompatible MEA with totally transparent electrodes made from PEDOT:PSS.

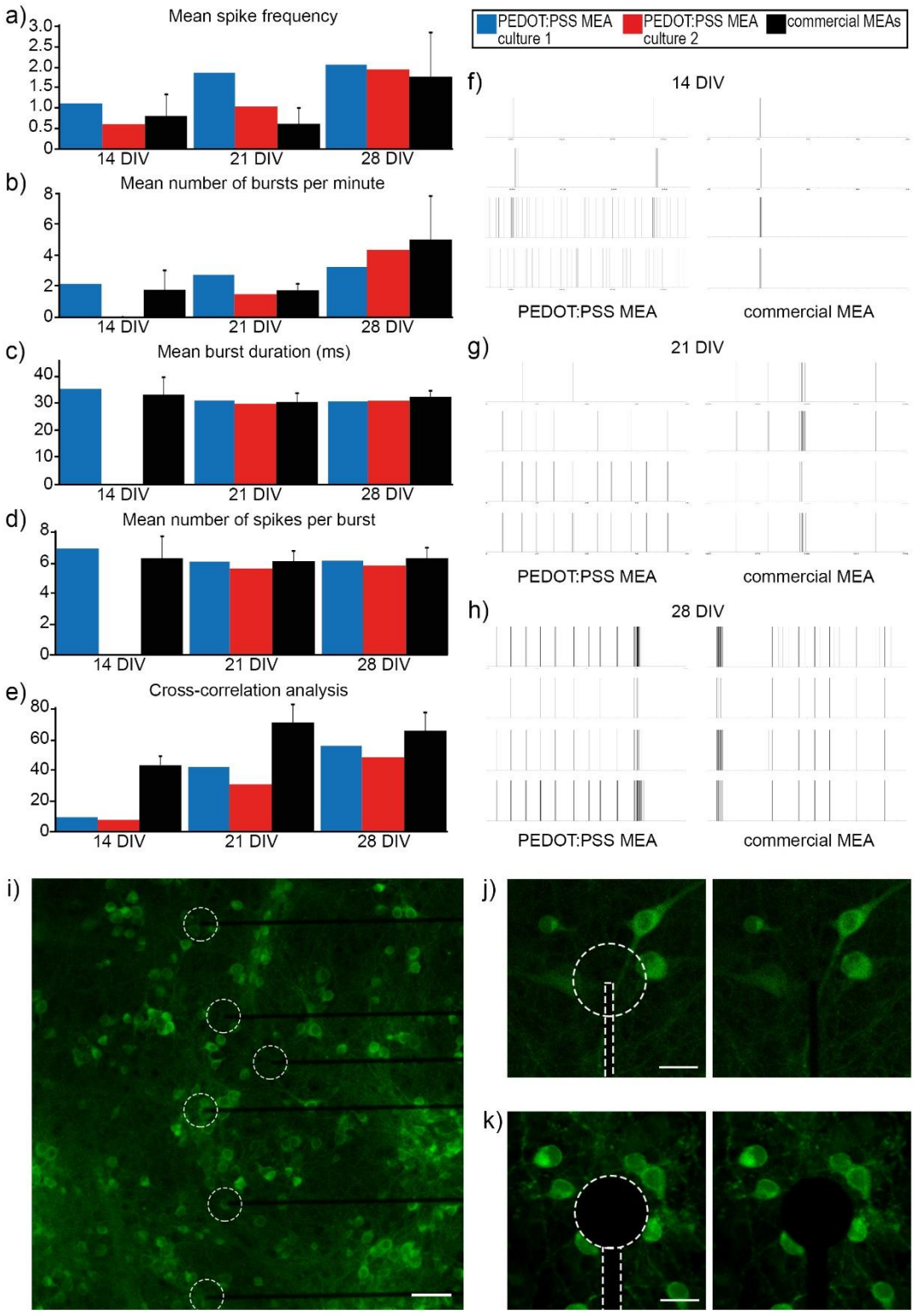

Fig. 5 Neuronal activity characterization and live-imaging of rat cortical cells cultured on a MEA with electrodes made from PEDOT:PSS compared to commercial MEAs with electrodes made of titanium nitride. Spontaneous neuronal activity was recorded after 14, 21 and 28 DIV. For commercial MEAs, $n = 3$ MEAs. The mean spike frequency (a), the mean number of bursts per minute (b), the mean burst duration in ms (c) the mean number of spikes per burst (d) and the results

of correlation analyses (e) are reported for each stage. Are also shown representative examples of extracellular traces **(timestamps)** of cortical networks cultured on both types of MEA **at 14 (f), 21 (g) and 28 (h) DIV**. The recording duration is 40 seconds and the recordings obtained from four nearby electrodes are displayed. Live-imaging of neurons on a MEA with totally transparent electrodes from PEDOT:PSS (i, j) and neurons on a commercial MEA that display opaque electrodes (made of titanium nitride) preventing us to image cells on top of them (k). Note that for MEA made with transparent electrodes from PEDOT:PSS, the connectors are opaque as they are made of titanium/gold. Scale bars, 20 µm (j, k) and 50 µm (i).

Conclusion

Our findings clearly demonstrate the viability of MEA technology for neuronal studies based on PEDOT:PSS microelectrodes. The devices were electrically characterized and showed high optical transmission (as high as 97%) and low electrical impedance values (33 MΩ μm^2)—comparable to the impedance of commercially available opaque MEA devices). The biocompatibility of PEDOT:PSS was also investigated and successfully validated, meaning that our approach is suitable for measuring signals from neurons. In addition, we have demonstrated that our systems were able to sustain neuron networks growing with maturation and synchronization after 4 weeks—and able to perform neuronal activity recording with a lower baseline noise compared to TiN-based commercial MEA. We were also able to live-image fluorescent-labelled neurons located on top of our PEDOT:PSS electrodes. Although MEA systems enable the extracellular recording of large populations of neuronal (or any other excitable or neuron-like cells) for weeks and even months; these recording could be less informative compared to intracellular ones. As most of MEA systems are composed by non-transparent electrodes, this prevents optical characterization of cells located on top of them, thus limiting the amount of additional information that can be obtained. For example, does the absence of signal from a given electrode come from absence of neurons, of living neurons, lack of neuronal activity or no neuronal activity triggering spike generation? Using our device, we showed that we could determine how many living neurons are present on top of the electrodes. In addition, other dyes sensitive to specific parameters (calcium concentration, reactive oxygen species, etc) can also be used to specifically assay the physiological state of the recorded cells. Moreover, a very important issue when working on neuronal networks is their complexity and potential cellular heterogeneity: this can be intrinsic to the model (for example cortical cells encompass different types of neurons) or induced by the experimenter to model a physiological or pathological situation. The use of fluorescent reporter genes (for example, genes specific to a type of neurons or other fluorescent markers can allow visualizing such heterogeneity. Thus, performing extracellular recording combined to a well-defined cell population is crucial to

conclude on the role of specific cells' status regarding the global network activity. Another advantage of our device is the possibility to perform optomodulation experiments (activation/inactivation of some functions) of our neuron network including both optogenetic and photochemical modulation (photoswitchable, photocleavable or drug release). Indeed, development of optomodulation tools in neuroscience are still growing, leading to device and probes able to perform simultaneously optical modulation and monitoring of neural activity. One of the very promising tool is, for instance, the genetically encoded voltage indicators (GEVI) system that has shown higher performances in terms of voltage detection sensibility over classical methods.

References

[1] D.A. Koutsouras, A. Hama, J. Pas, P. Gkoupidenis, E.N. Supérieure, PEDOT : PSS microelectrode arrays for hippocampal cell culture electrophysiological recordings, 7 (2017) 259–265. https://doi.org/10.1557/mrc.2017.34.

[2] Y. Nam, B.C. Wheeler, In Vitro Microelectrode Array Technology and Neural Recordings, 39 (2011) 45–61.

[3] P. Kshirsagar, S. Dickreuter, M. Mierzejewski, C.J. Burkhardt, T. Chassé, M. Fleischer, P.D. Jones, Transparent Graphene / PEDOT : PSS Microelectrodes for Electro- and Optophysiology, 1800318 (2019) 1–7. https://doi.org/10.1002/admt.201800318.

[4] R. Gerwig, K. Fuchsberger, B. Schroeppel, G.S. Link, G. Heusel, U. Kraushaar, W. Schuhmann, A. Stett, M. Stelzle, PEDOT – CNT composite microelectrodes for recording and electrostimulation applications : fabrication , morphology , and electrical properties, 5 (2012) 1–11. https://doi.org/10.3389/fneng.2012.00008.

[5] M. Sessolo, D. Khodagholy, J. Rivnay, F. Maddalena, M. Gleyzes, E. Steidl, B. Buisson, G.G. Malliaras, Easy-to-Fabricate Conducting Polymer Microelectrode Arrays, (2013) 2135–2139. https://doi.org/10.1002/adma.201204322.

[6] E.M. Steidl, E. Neveu, D. Bertrand, B. Buisson, The adult rat hippocampal slice revisited with multi-electrode arrays, Brain Research. (2006). https://doi.org/10.1016/j.brainres.2006.04.034.

[7] Www.multichannelsystems.com, Microsoft, Microelectrode Array (MEA) Manual, in: Multi Channel Systems MCS GmbH, 2019.

[8] M.N. Solovan, V. V Brus, E. V Maistruk, P.D. Maryanchuk, Electrical and Optical Properties of TiN Thin Films, (2014). https://doi.org/10.1134/S0020168514010178.

[9] T. Ryynänen, A. Pelkonen, K. Grigoras, O.M.E. Ylivaara, Microelectrode Array With Transparent ALD TiN Electrodes, 13 (2019) 1–7. https://doi.org/10.3389/fnins.2019.00226.

[10] W. Lee, D. Kim, N. Matsuhisa, M. Nagase, M. Sekino, G.G. Malliaras, T. Yokota, T. Someya, Transparent, conformable, active multielectrode array using organic

electrochemical transistors, Proceedings of the National Academy of Sciences of the United States of America. 114 (2017) 10554–10559. https://doi.org/10.1073/pnas.1703886114.

[11] K.Y. Kwon, S. Member, B. Sirowatka, A. Weber, W. Li, Opto- Array : A Hybrid Neural Interface With Transparent Electrode Array and Integrated LEDs for Optogenetics, 7 (2013) 593–600.

[12] X. Du, L. Wu, J. Cheng, S. Huang, Graphene microelectrode arrays for neural activity detection, (2015) 339–347. https://doi.org/10.1007/s10867-015-9382-3.

[13] D. Kuzum, H. Takano, E. Shim, J.C. Reed, H. Juul, A.G. Richardson, J. De Vries, H. Bink, M.A. Dichter, T.H. Lucas, D.A. Coulter, E. Cubukcu, B. Litt, Transparent and flexible low noise graphene electrodes for simultaneous electrophysiology and neuroimaging, Nature Communications. 5 (2014) 1–10. https://doi.org/10.1038/ncomms6259.

[14] D. Park, A.A. Schendel, S. Mikael, S.K. Brodnick, T.J. Richner, J.P. Ness, M.R. Hayat, F. Atry, S.T. Frye, R. Pashaie, S. Thongpang, Z. Ma, J.C. Williams, applications, Nature Communications. 5 (2014) 1–11. https://doi.org/10.1038/ncomms6258.

[15] T. Ryynänen, M. Pekkanen-Mattila, D. Shah, J. Kreutzer, P. Kallio, J. Lekkala, K. Aalto-Setälä, Microelectrode array for noninvasive analysis of cardiomyocytes at the single-cell level, Japanese Journal of Applied Physics. 57 (2018). https://doi.org/10.7567/JJAP.57.117001.

[16] P. Kshirsagar, M. Martina, P.D. Jones, S. Buckenmaier, U. Kraushaar, T. Chassé, M. Fleischer, C.J. Burkhardt, Semitransparent carbon microelectrodes for opto- and electrophysiology, Journal of Micromechanics and Microengineering. 28 (2018). https://doi.org/10.1088/1361-6439/aab9f0.

[17] M. Ganji, E. Kaestner, J. Hermiz, N. Rogers, A. Tanaka, D. Cleary, S.H. Lee, J. Snider, M. Halgren, G.R. Cosgrove, B.S. Carter, D. Barba, I. Uguz, G.G. Malliaras, S.S. Cash, V. Gilja, E. Halgren, S.A. Dayeh, Development and Translation of PEDOT : PSS Microelectrodes for Intraoperative Monitoring, 1700232 (2017) 1–11. https://doi.org/10.1002/adfm.201700232.

[18] L. Groenendaal, F. Jonas, D. Freitag, H. Pielartzik, J.R. Reynolds, Poly(3,4-ethylenedioxythiophene) and its derivatives: past, present, and future, Advanced Materials. 12 (2000) 481–494. https://doi.org/10.1002/(SICI)1521-4095(200004)12:7<481::AID-ADMA481>3.0.CO;2-C.

[19] D.-J. Kim, N.-E. Lee, J.-S. Park, I.-J. Park, J.-G. Kim, H.J. Cho, Organic electrochemical transistor based immunosensor for prostate specific antigen (PSA) detection using gold nanoparticles for signal amplification., Biosensors & Bioelectronics. 25 (2010) 2477–82. https://doi.org/10.1016/j.bios.2010.04.013.

[20] S.M. Kim, N. Kim, Y. Kim, M.S. Baik, M. Yoo, D. Kim, W.J. Lee, D.H. Kang, S. Kim, K. Lee, M.H. Yoon, High-performance, polymer-based direct cellular interfaces for electrical stimulation and recording, NPG Asia Materials. 10 (2018) 255–265. https://doi.org/10.1038/s41427-018-0014-9.

[21] J. Pas, C. Pitsalidis, D.A. Koutsouras, P.P. Quilichini, F. Santoro, B. Cui, L. Gallais,

R.P.O. Connor, G.G. Malliaras, R.M. Owens, Neurospheres on Patterned PEDOT : PSS Microelectrode Arrays Enhance Electrophysiology Recordings, 1700164 (2018) 1–11. https://doi.org/10.1002/adbi.201700164.

[22] D. Khodagholy, T. Doublet, M. Gurfi, P. Quilichini, E. Ismailova, P. Leleux, T. Herve, S. Sanaur, C. Bernard, G.G. Malliaras, Highly Conformable Conducting Polymer Electrodes for In Vivo Recordings, (2011) 268–272. https://doi.org/10.1002/adma.201102378.

[23] L.D. Garma, L.M. Ferrari, P. Scognamiglio, F. Greco, F. Santoro, Lab on a Chip, (2019). https://doi.org/10.1039/c9lc00636b.

[24] Www.multichannelsystems.com, Microsoft, Microelectrode Array (MEA) Manual, in: Multi Channel Systems MCS GmbH, 2013.

[25] J. Rivnay, P. Leleux, M. Ferro, M. Sessolo, A. Williamson, D.A. Koutsouras, D. Khodagholy, M. Ramuz, X. Strakosas, R.M. Owens, C. Benar, J. Badier, C. Bernard, G.G. Malliaras, High-performance transistors for bioelectronics through tuning of channel thickness, (2015) 1–6.

[26] K.Y. Kwon, S. Member, B. Sirowatka, A. Weber, W. Li, Opto - μECoG Array : A Hybrid Neural Interface with Transparent μECoG Electrode Array and Integrated LEDs for Optogenetics, (2013) 1–8.

[27] D. Ito, T. Komatsu, K. Gohara, Measurement of saturation processes in glutamatergic and GABAergic synapse densities during long-term development of cultured rat cortical networks, Brain Research. 1534 (2013) 22–32. https://doi.org/10.1016/j.brainres.2013.08.004.

[28] D.A. Wagenaar, J. Pine, S.M. Potter, An extremely rich repertoire of bursting patterns during the development of cortical cultures, BMC Neuroscience. 7 (2006) 1–18. https://doi.org/10.1186/1471-2202-7-11.

Acknowledgements

We acknowledge the Labex DistalZ project (Development of Innovative Strategies for a Transdisciplinary approach to ALZheimer's disease), the EU: ERC-2017-COG project IONOS (# GA 773228), the University of Lille, CNRS and PEpS project for financial support. This work was also partly supported by the French RENATECH network (French national nanofabrication platform).